Bridging the Analog and the Probabilistic Computing Divide: Configuring Oscillator Ising Machines as P-bit Engines

E.M.H.E.B. Ekanayake, Nikhat Khan, and Nikhil Shukla

University of Virginia, Charlottesville, VA, USA

Oscillator Ising Machines (OIMs) and probabilistic bit (p-bit)-based computing platforms have emerged as promising paradigms for tackling complex combinatorial optimization problems. Although traditionally viewed as distinct approaches, this work presents a theoretically grounded framework for configuring OIMs as p-bit engines. We demonstrate that this functionality can be enabled through a novel interplay between first- and second harmonic injection to the oscillators. Our work identifies new synergies between the two methods and broadens the scope of applications for OIMs. We further show that the proposed approach can be applied to other analog dynamical systems, such as the Dynamical Ising Machine.

I. INTRODUCTION

The endeavor to devise efficient solutions to complex computational problems has been a longstanding focus of science and technology research owing to its far-reaching implications for practical applications. A recent example of such an effort has been the focus on solving complex combinatorial optimization problems (COPs) which form the backbone of many practical applications ranging from protein folding, scheduling tasks to portfolio optimization. An archetypal COP that serves as a good benchmark for such efforts is the minimization of the Ising Hamiltonian. The problem can be defined as the goal of finding a spin configuration $s \in \{-1, +1\}$ that minimizes the Ising Hamiltonian given by $H = -\sum J_{ij}s_is_j$, where J_{ij} is the interaction between spin i and spin j. In recent years, innovative hardware-based methods [1] that go beyond traditional heuristics have emerged, that aim to solve this problem with increased energy efficiency and performance. Such approaches span the optical [2, 3], acoustic [4], electronic [5–10], spin [11], and quantum domains [12]. The eventual goal of these efforts is to enable the design of the so-called Ising machines, which can be considered as special purpose accelerators capable of minimizing the Ising Hamiltonian with transformative gains in performance.

In this context, two complementary methods, namely analog oscillator Ising machines (OIMs) and probabilistic bit (p-bit)-based computing platforms have emerged as potential contenders. OIMs, first proposed by Wang *et al.* [13] exploit the elegant equivalence between the 'energy function' characterizing the dynamics of a network of coupled oscillators under second harmonic injection (SHI) and the Ising Hamiltonian. Consequently, under the right set of parameters [14–16], as the physical system of oscillators evolves to reduce its energy, it naturally computes the solution to the problem.

P-bit-based computing, with its foundation rooted in Markov Chain Monte Carlo (MCMC) sampling, presents a complementary paradigm for designing Ising machines [17–24]. The fundamental idea of the p-bit lies in realizing a random number generator with a tunable probability distribution. P-bit engines can be considered as binary stochastic neural networks (BSNNs) [25] where the probability of a spin state is governed by the synaptic input. This behavior can be captured by the state update rule wherein the updated state of the ith spin is given by,

$$s_i^+ = \text{sgn}\left[\tanh\left(\beta \sum_{\substack{j=1 \\ j\neq i}}^{N} J_{ij}s_j\right) - \mu\right] \quad (1)$$

where, μ is a random number typically selected from a uniform distribution between $[-1, 1]$, and β is the equivalent of inverse temperature [26]. Furthermore, if we interpret the spins as the phases of oscillators—a perspective that is useful in the context of this work—then the state update rule can be expressed as,

$$s_i^+ = \cos\phi_i = \text{sgn}\left[\tanh\left(\beta \sum_{\substack{j=1 \\ j\neq i}}^{N} J_{ij}\cos\phi_j\right) - \mu\right] \quad (2)$$

where, $\phi \in \{0, \pi\}$ (wrapped phase form). In both Eqs. (1) and (2), the self bias term has not been considered although it is relatively straightforward to include it into the approach presented here. Traditionally, OIMs and p-bit-based computing platforms have been pursued as largely independent approaches, with limited investigation into their potential synergies [27, 28]. In this work, we explore a novel intersection of these paradigms by demonstrating the feasibility of configuring OIMs as p-bit engines. This approach not only offers an analog alternative that circumvents the need for digital feedback circuitry typically required in conventional p-bit implementations, but also broadens the functional scope of OIMs. Specifically, it establishes a pathway for employing OIMs in applications that entail sampling such as training restricted Boltzmann machines (RBMs), thereby extending their utility beyond traditional combinatorial optimization tasks.

To establish the foundation of our oscillator-based p-bit engine, we begin by demonstrating two key properties of harmonic oscillators (the class of harmonic oscillators
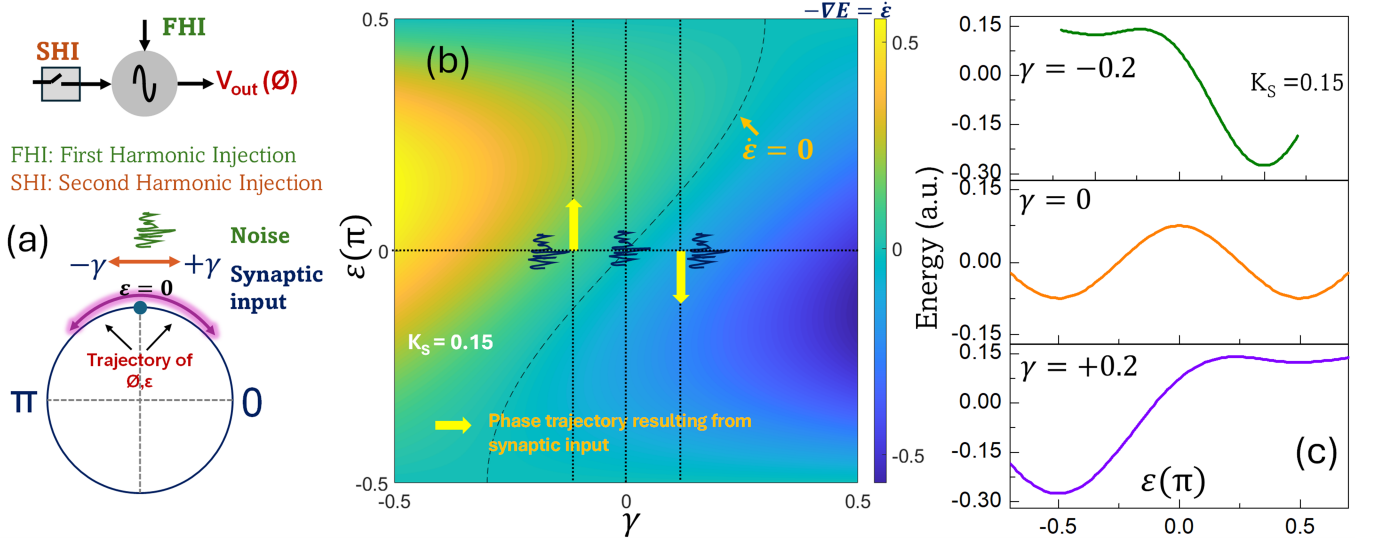
Figure 1: **Dynamics of a harmonic oscillator under SHI** (a) Schematic illustration of the signals required to program an oscillator as a p-bit. (b) Force field as a function of γ ($K_s = 0.15$). (c) Evolution of the energy landscape of the oscillator as a function of γ ($K_s = 0.15$).

considered in this study) and their networks operating under SHI: (a) An oscillator subjected to first- and second harmonic injection can function as a binary stochastic neuron (BSN); and (b) A network of such coupled oscillators—specifically an OIM—can operate as a binary stochastic neural network (BSNN). These two properties form the conceptual and mathematical basis for designing an oscillator-based p-bit engine.

II. CONFIGURING OSCILLATORS AS STOCHASTIC NEURONS

To design a binary stochastic neuron (BSN) using an oscillator, we first examine the dynamics of a harmonic oscillator subjected to two external inputs (Fig. 1(a)). **(a)** The first input is a signal with a frequency nearly equal to the oscillator's natural frequency—a condition commonly referred to as injection locking. Within a specific locking range, this external signal entrains the oscillator, steering its output toward the phase and frequency of the injected signal, effectively synchronizing the oscillator's behavior with the input. An energetics-based explanation of the relevant phase behavior is provided in Appendix A. We refer to this signal as the fundamental harmonic injection (FHI). All phase values are defined with respect to a common reference signal. **(b)** The second input is SHI, operating at twice the oscillator's natural frequency. SHI drives the oscillator phase toward either $\phi = 0$ or $\phi = \pi$.

The resulting phase dynamics of such an oscillator can be described by,

$$\frac{d\phi}{dt} = -K_c \sin(\phi - \theta) - K_s \sin(2\phi) \tag{3}$$

where, ϕ denotes the output phase of the oscillator, while θ represents the phase offset of the FHI signal input. The parameters K_c and K_s are coupling constants of the FHI and SHI signals, with the first and the second terms on the RHS of Eq. (3) capturing the influence of the FHI and SHI, respectively.

In this work, we will restrict our attention to cases where $\theta \in \{0, \frac{\pi}{2}, \pi\}$. Initially, we will focus on the analysis where $\theta \in \{0, \pi\}$, with the case $\theta = \frac{\pi}{2}$ becoming relevant further on. Under this constraint, we can recast Eq. (3) as,

$$\frac{d\phi}{dt} = -\gamma \sin(\phi) - K_s \sin(2\phi) \tag{4}$$

where, γ ($= K_c$) denotes a scaled version of the synaptic input. For simplicity, we will generally refer to γ as the synaptic input in the following discussion. The details of the scaling factor will be elaborated in the subsequent section.

Furthermore, for convenience, we perform a frame rotation by 0.5π, redefining the phase as $\phi = \frac{\pi}{2} + \epsilon$. We also note that the relevant values of θ for this rotated frame shift to $\theta' \in \{-\frac{\pi}{2}, 0, \frac{\pi}{2}\}$. Under this transformation, equation (4) becomes,

$$\frac{d\epsilon}{dt} = -\gamma \cos(\epsilon) + K_s \sin(2\epsilon) \tag{5}$$

We now analyze the properties and the behavior of Eq. (5). First, the fixed points of this system lie at

$\epsilon_1^* = \pm 0.5\pi$, and at values satisfying $\sin(\epsilon_2^*) = \frac{\gamma}{2K_s}$. A detailed stability analysis of all the fixed points has been presented in Appendix B.

Next, we investigate the expected dynamical behavior of the system by analyzing the effective force field $(-\nabla E = \dot{\epsilon})$ driving the phase evolution as a function of γ, as shown in Fig. 1(b). The dotted line in the figure represents the set of phase points where the phase velocity vanishes, i.e., $\frac{d\epsilon}{dt} = 0$, and is described by the equation:

$$-\gamma + 2K_s \sin(\epsilon) = 0$$

This curve defines the *nullcline* of the system, separating regions of positive and negative phase flow.

Interestingly, when the system is initialized at $\epsilon = 0$, the direction of phase evolution depends entirely on the sign of γ. For $\gamma < 0$, the dynamics flow toward $\epsilon = \frac{\pi}{2}$ (corresponding to $\phi = \pi$). Conversely, for $\gamma > 0$, the dynamics flow toward $\epsilon = -\frac{\pi}{2}$ (i.e., $\phi = 0$). Moreover, the magnitude of γ determines the steepness of the phase flow at $\epsilon = 0$. At the critical point $\gamma = 0$, the direction of phase evolution becomes entirely stochastic in the presence of noise.

Figure 1(c) shows the evolution of the oscillator's energy landscape for different values of γ, illustrating how the energy evolves with the synaptic input. The relative symmetry about $\epsilon = 0$ is evident across all cases, with the energy profiles for $\gamma = \pm 0.2$ appearing as mirror images, and the $\gamma = 0$ case exhibiting a perfectly symmetric landscape.

In alignment with prior work on magnetic tunnel junctions (MTJs)-based p-bits [29], we engineer our oscillator-based BSN to operate within the low energy barrier regime. Since the height of the barrier is controlled by K_s (see Appendix C for details), this is achieved by tuning K_s to a small value ($K_s \ll 1$). Thus, the oscillator-based approach can enable a BSN with a tunable barrier.

From 1(b) as well as from the form of Eq. (5), it can be observed that the system exhibits a unique symmetry at $\epsilon = 0$, within the domain $\epsilon \in \left[-\frac{\pi}{2}, \frac{\pi}{2}\right]$, whereby the magnitude of the (scaled) synaptic input has a symmetric effect for $+\gamma$ and $-\gamma$, but induces phase flows in opposite directions. This symmetry plays a critical role in enabling the oscillator to function as a BSN, as it defines a neutral point from which the system can stochastically evolve toward one of two stable states depending on the sign of the synaptic input. As we will show later, this stochastic response is also highly non-linear. In practical settings, the oscillator can be driven to this neutral point $\epsilon = 0$ using an FHI signal with a phase offset of $\epsilon = 0$ (we refer to this input as FHI^0), and without applying the SHI.

Thus, operating the oscillator as a BSN entails the following steps:

(i) Set oscillator phase to the neutral point using FHI^0.

(ii) Remove FHI^0 followed by application of the synaptic input (also an FHI signal) and SHI signal (applied as a ramp) to evaluate the (stochastic) neuron's state—this constitutes a sampling event. As we will demonstrate later, in the OIM network, such synaptic input is effectively generated by other connected oscillators within the network.

III. DYNAMICS OF AN OSCILLATOR-BASED BSN

To quantitatively analyze the stochastic nonlinear response of the oscillator-based BSN, we begin with the oscillator dynamics described in Eq. (5). We first define the updated spin state in terms of ϵ, which, in the context of the continuous time dynamics considered here, is given by,

$$s^+ = \text{sgn}\left(\cos(\phi^+)\right) = -\text{sgn}\left(\sin(\epsilon^+)\right)$$

where, ϕ^+ and ϵ^+ refer to the phase of the system at a small time increment $\Delta t \to 0$ after the sampling has been initiated.

We now evaluate the solution to the dynamics presented in Eq. (5). Although deriving an explicit solution is challenging, Eq. (5) has an implicit analytical solution given by,

$$\frac{\zeta(\epsilon) - \gamma \tanh^{-1}(\sin(\epsilon))}{\gamma^2 - 4K_s^2} = t \quad (6)$$

where,

$$\zeta(\epsilon) = K_s\big(-2\log(\gamma - 2K_s\sin(\epsilon)) + \log(1 - \sin(\epsilon)) + \log(\sin(\epsilon) + 1)\big)$$

For it's applications as a BSN, we focus on the direction of the initial phase trajectory. To understand and evaluate the system dynamics at the sampling instant—defined as the moment when (FHI^0) is suppressed and the SHI and the synaptic input are asserted—we adopt the following approximation:

(i) The dynamics are evaluated in the limit $t \to 0$.

(ii) We model the noise as Gaussian white noise with $\langle \eta(t) \rangle = 0$, $\langle \eta(t)\eta(t') \rangle = 2K_n\delta(t - t')$, with K_n denoting the noise intensity i.e., $\eta(t)\,dt = \sqrt{2K_n}\,dW_t$, where W_t is a Wiener process. Equivalently, over a finite timestep Δt, $\int_t^{t+\Delta t} \eta(\tau)\,d\tau \sim \mathcal{N}(0, 2K_n\,\Delta t)$.

(iii) At the onset of sampling $(t \to 0)$, we assume $K_s \to 0$ such that $K_s \ll |\gamma|$. This reflects the requirement for a low energy barrier in the probabilistic regime. Subsequently, K_s must be ramped up for reasons discussed in the following section.

Under these approximations, the oscillator phase can be expressed as:

$$\sin(\epsilon_i) \approx \tanh\left(-\gamma t + \epsilon^\eta(t)\right)$$

$$\approx \tanh\left(-\gamma t\right) + \epsilon^\eta(t).\text{sech}^2(\gamma t) \qquad (7)$$

Here, $\epsilon^\eta(t) \sim \mathcal{N}\left(0, 2K_n t\right)$, and is small such that the tanh(.) term can be linearized. Accordingly, at a small time increment $\Delta t \to 0$ after the onset of sampling at t=0, the updated state of the oscillator-based BSN can be described as,

$$s^+ \approx \text{sgn}\left[\tanh(\gamma\Delta t) - \epsilon^\eta(\Delta t).\text{sech}^2(\gamma\Delta t)\right] \qquad (8)$$

$$\equiv \text{sgn}\left[\tanh(\gamma\Delta t) - \vartheta\right]$$

where, $\vartheta \equiv \epsilon^\eta(\Delta t).\text{sech}^2(\gamma\Delta t)$. Since $\text{sech}^2(\gamma\Delta t) \in (0,1]$, and noise intensity is assumed to be small, ϑ has a high probability of being in the interval [-1,+1]. The derivation of Eqs. (7) and (8) has been presented in Appendix D. Furthermore, while Eq. (7) addresses the regime where $\gamma \gg K_s$, we also consider (in Appendix D) the complementary case where both γ and K_s are small and comparable. In this setting, the synaptic bias γ and the stochastic perturbations act as competing drivers of the phase dynamics. A large $|\gamma|$ produces a predictable exponential drift, whereas strong noise leads to rapid amplification of fluctuations and broad dispersion of trajectories. The observed evolution is therefore governed by the balance between deterministic drive and stochastic forcing.

We note that the actual synaptic input to the BSN would be applied as the voltage (or current) amplitude of the injected signal, V_{inj}, which relates to γ and the coupling constant K_c as $\gamma = K_c \approx \frac{\omega_0}{2Q} \cdot \frac{V_{\text{inj}}}{V_{\text{osc}}}$ [30, 31], where Q is the quality factor of the oscillator, ω_0 is the natural frequency, and V_{inj} and V_{osc} represent the amplitude of the injection signal and the oscillator, respectively. This formulation implies that γ serves as a scaled representation of the synaptic input, as noted earlier. Furthermore, the effective inverse temperature is then given by $\beta_{\text{eff}} = \frac{\omega_0 \Delta t}{2V_{\text{osc}}} \frac{1}{Q}$ implying that β_{eff} can be modulated using the quality factor, Q, of the oscillator as well as other parameters such as the oscillation amplitude. This tunability provides a practical mechanism for controlling the stochastic behavior of the system. The updated state is then expressed as

$$s^+ \approx \text{sgn}\left[\tanh\left(\frac{\omega_0 \Delta t}{2QV_{\text{osc}}} \cdot V_{\text{inj}}\right) - \vartheta\right] \qquad (9)$$

$$\equiv \text{sgn}\left[\tanh\left(\beta_{\text{eff}} \cdot V_{\text{inj}}\right) - \vartheta\right]$$

Equation (9) showcases the BSN's capability to perform Boltzmann sampling, and consequently, function as
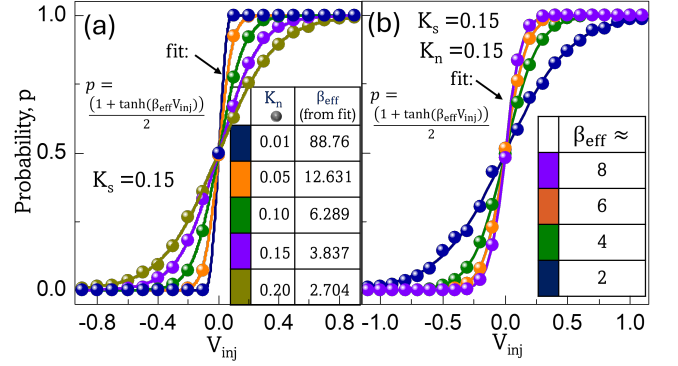

Figure 2: **Oscillator-based BSN.** Firing probability (symbols) as a function of the synaptic input for: (a) varying levels of noise (K_n). (b) different values of β_{eff} derived for $K_n = 0.15$. We note that the β_{eff} profile will change for a different K_n. The lines in the plot indicate fits using the equation $p = \frac{1+\tanh(\beta_{\text{eff}}V_{\text{inj}})}{2}$ along with the calculated β_{eff}; p : firing probability All fits exhibit $R^2 > 0.999$

a p-bit when initialized at the critical phase point, $\epsilon = 0$. To validate the dynamics derived above, we simulate the oscillator-based BSN's switching using a stochastic differential equation solver implemented in MATLAB®. We first examine the evolution of stochastic behavior under varying noise levels. The phase is initialized at $\epsilon = 0$ and allowed to evolve in the presence of different noise intensities and synaptic inputs. The firing probability is then estimated over 2000 such cycles. Figure 2(a) presents the simulation results (symbols) for the output firing probability of the oscillator-based BSN as a function of V_{inj}. These results are fitted using the function $p = \frac{1+\tanh(\beta_{\text{eff}}V_{\text{inj}})}{2}$ (solid lines), showing excellent agreement with the simulated data ($R^2 > 0.999$); p is the probability of the neuron firing i.e., switching to $s = +1$.

In practical implementations, modulating external noise to control temperature and stochasticity may not be feasible. Instead, the effective inverse temperature—and thus the degree of stochastic behavior—can be tuned by adjusting β_{eff}, which is achievable through modulation of the oscillator's quality factor Q. Figure 2(b) illustrates the evolution of firing probability (symbols) for different values of β_{eff}, where the switching probability again exhibits tanh(.) dependence on V_{inj} as confirmed by the corresponding fitted curves (solid lines) with $R^2 > 0.999$. A noise strength of $K_n = 0.15$ was used in the simulation. These simulation results further support that the oscillator exhibits the characteristic behavior of a BSN capable of performing Boltzmann sampling.

A key consideration in engineering the oscillator's dynamics for BSN functionality is the relative magnitude of γ and the SHI strength, K_s. Realizing effective Boltzmann sampling behavior requires a small energy bar-

rier, which corresponds to the regime $K_s \to 0$ such that $K_s \ll |\gamma|$. If this condition is not satisfied, the system may still operate as a BSN; however, its dynamics may deviate from the Boltzmann sampling behavior. This is detailed in the analysis in Appendix D.

In contrast, to preserve the oscillator's phase trajectory after sampling and to enable reliable readout, a lower bound on K_s must be satisfied. Specifically, this bound ensures that once the phase magnitude exceeds a certain threshold ($|\epsilon_{th}|$), the phase continues to evolve in the same direction until it reaches the corresponding fixed point.

While a detailed analytical derivation is provided in Appendix E, we offer here a qualitative explanation of the origin of this constraint by examining the dynamics described by Eq. (5). Within the interval $\epsilon \in (-\frac{\pi}{2}, \frac{\pi}{2})$, the cosine term satisfies $\cos(\epsilon) > 0$, and the synaptic input term $-\gamma \cos(\epsilon)$ therefore drives the phase evolution in the direction *opposite* to the sign of γ. This implies that the synaptic input alone tends to push the phase toward the fixed point opposite to the sign of γ, unless counteracted by the SHI term.

If noise initially drives $\frac{d\epsilon}{dt}$ in the direction not favored by the synaptic input (Fig.6(b)), and K_s is too small, the oscillator may reverse its trajectory *to align with the trajectory favored by the synaptic input.* In such cases, the final state may not reflect the oscillator's initial trajectory or the intended output s^+. The SHI term— specifically, the $K_s \sin(2\epsilon)$ component in Eq. (5), acts to reinforce the initial direction of $\frac{d\epsilon}{dt}$ *generated by the stochastic sampling process*, provided K_s is sufficiently large. This reinforcement helps ensure that the phase continues toward the correct fixed point.

The critical condition to ensure that an oscillator at $\epsilon = |\epsilon_{th}|$ maintains its trajectory is given by:

$$|\gamma| < 2K_s \sin(|\epsilon_{th}|)$$

It is important to note that due to the presence of noise, this threshold is inherently probabilistic, resulting in a diffuse rather than deterministic boundary.

This condition appears to contradict the earlier requirement concerning the relative magnitudes of γ and K_s. To reconcile these seemingly opposing constraints, we propose implementing the SHI input as a ramp signal with a carefully engineered slew rate. Specifically, the SHI can be initialized at a low amplitude—ensuring that $K_s \ll |\gamma|$—to facilitate stochastic sampling in the low-barrier regime. Subsequently, the amplitude of the SHI is increased to reinforce the resulting phase trajectory.

IV. CONFIGURING OIMs AS BINARY STOCHASTIC NEURAL NETWORKS

Building upon the ability to configure an oscillator as a BSN capable of performing Boltzmann sampling, we now investigate the possibility of configuring an OIM as a p-bit engine, or in other words, a BSNN. The core premise

of this idea is that *after* the system reaches steady state, i.e., $\epsilon \in \{-\frac{\pi}{2}, \frac{\pi}{2}\}$, the dynamics of a randomly sampled oscillator driven to the phase point $\epsilon = 0$ (i.e., $\phi = \frac{\pi}{2}$) still approximate Boltzmann sampling. Interestingly, in the OIM, the feedback from other coupled oscillators acts as the effective synaptic input, which subsequently modulates the oscillator's stochastic dynamics.

To establish this result, in the following sections, we divide the oscillators in the network into two categories and analyze their dynamics:

(i) Randomly sampled oscillator i initialized to $\epsilon_i = 0$.

The phase evolution of an oscillator in the OIM network can be described by the equation,

$$\frac{d\phi_i}{dt} = -K \sum_{\substack{j=1 \\ j \neq i}}^{N} J_{ij} \sin(\phi_i - \phi_j) - K_s \sin(2\phi_i)$$

which, in the rotated frame of reference, can be expressed as,

$$\frac{d\epsilon_i}{dt} = -K \sum_{\substack{j=1 \\ j \neq i}}^{N} J_{ij} \sin(\epsilon_i - \epsilon_j) + K_s \sin(2\epsilon_i) \qquad (10)$$

As alluded to earlier, we assume that:

(i) The selected oscillator is initialized at $\epsilon = 0$. This can be accomplished using FHI^0 signal with large amplitude.

(ii) Since we begin performing stochastic sampling after the OIM network has achieved steady state, all *other* oscillators are at $\epsilon = \pm\frac{\pi}{2}$ $(\phi \in \{0, \pi\})$. Furthermore, we will ensure that the oscillators maintain their state during the sampling event by applying a sufficiently large K_s. In the subsequent sections, we will discuss how these conditions can be implemented.

Under the constraints outlined above, the phase dynamics of the selected oscillator simplify to:

$$\frac{d\epsilon_i}{dt} = \left(K \sum_{\substack{j=1 \\ j \neq i}}^{N} J_{ij} \sin(\epsilon_j) \right) \cos(\epsilon_i) + K_s \sin(2\epsilon_i) \tag{11}$$

$$\equiv -\gamma_i \cos(\epsilon_i) + K_s \sin(2\epsilon_i)$$

where,

$$\gamma_i = -K \sum_{\substack{j=1 \\ j \neq i}}^{N} J_{ij} \sin(\epsilon_j)$$

We now show that γ_i, as defined above, represents the synaptic input to oscillator i from the other connected oscillators in the network. To establish this, we consider the relationship between ϵ and ϕ, and the fact that $s = \cos(\phi)$ when $\phi \in \{0, \pi\}$:

$$\gamma_i = -K \sum_{\substack{j=1 \\ j \neq i}}^{N} J_{ij} \sin(\epsilon_j) = -K \sum_{\substack{j=1 \\ j \neq i}}^{N} J_{ij} \sin\left(\phi_j - \frac{\pi}{2}\right)$$

$$= K \sum_{\substack{j=1 \\ j \neq i}}^{N} J_{ij} \cos(\phi_j) = K \sum_{\substack{j=1 \\ j \neq i}}^{N} J_{ij} s_j$$

This establishes that γ_i represents the net synaptic input received by oscillator i from the connected oscillators under the conditions described above. Additionally, we note that the self-biasing term can be incorporated by injecting an FHI signal to oscillator with the strength and phase of the signal representing the self-bias input.

The updated state of oscillator i can then be expressed as,

$$s_i^+ \approx -\text{sgn}\left[\tanh(-\gamma_i \Delta t) + \epsilon^\eta(\Delta t).\text{sech}^2(\gamma \Delta t)\right]$$

$$\approx \text{sgn}\left[\tanh\left(K\Delta t \sum_{\substack{j=1 \\ j \neq i}}^{N} J_{ij} s_j\right) - \vartheta\right] \tag{12}$$

which closely resembles the state update rule for p-bits (Eq. (1)), with the factor $\beta_{\text{eff}} = K\Delta t$ serving as the effective inverse temperature. As detailed in [13], the value of K depends on the perturbation projection vector function for the oscillator as well as the amplitude of the perturbation from the oscillators in the network, which can be tuned via the coupling element in the network. This equivalence implies that even in the OIM, the oscillator can approximate Boltzmann sampling thereby enabling the network to function as a p-bit platform.

One of the critical requirements of realizing the above dynamics is to drive the randomly selected oscillator i to $\epsilon_i = 0$ $\left(\phi_i = \frac{\pi}{2}\right)$. This can be achieved by applying a large FHI signal, FHI^0, while suppressing the SHI signal ($K_s = 0$). The resulting dynamics can be described by:

$$\frac{d\epsilon_i}{dt} = -K_{c,i} \sin(\epsilon_i) - K \sum_{\substack{j=1 \\ j \neq i}}^{N} J_{ij} \sin(\epsilon_i - \epsilon_j) \tag{13}$$

The largest magnitude of the second term is D_i—the degree of the node (oscillator) i in the network. By designing $K_{c,i} \gg KD_i$ ensures that the contributions of the second term are small. Consequently, the phase will be driven to $\epsilon_i \approx 0$, thereby preparing it for the subsequent stochastic sampling event.

(ii) Oscillators not being sampled

Under steady state, such oscillators have phases $\epsilon = \pm\frac{\pi}{2}$, and the goal is to maintain the configuration when oscillator i is sampled. To achieve this, we apply a strong SHI signal. The corresponding dynamics for an oscillator j that is not being sampled can be then described as follows:

$$\frac{d\epsilon_j}{dt} = -K \sum_{\substack{k=1 \\ k \neq j}}^{N} J_{jk} \sin(\epsilon_j - \epsilon_k) + K_s \sin(2\epsilon_j) \tag{14}$$

$$\forall j \in \{1, 2, \ldots, i-1, i+1, \ldots, N\}$$

Furthermore, $\sin(\epsilon_j - \epsilon_k) \approx 0$ since

$$\epsilon_k \in \left\{-\frac{\pi}{2}, \frac{\pi}{2}\right\} \quad \forall j, k \in \{1, 2, \ldots, i-1, i+1, \ldots, N\}$$

Consequently, the dynamics can be reduced to,

$$\frac{d\epsilon_j}{dt} = -KJ_{ji} \sin(\epsilon_j - \epsilon_i) + K_s \sin(2\epsilon_j) \tag{15}$$

$$\forall j \in \{1, 2, \ldots, i-1, i+1, \ldots, N\}$$

The maximum magnitude of the first term is $|KJ_{ji}|$. Thus, by using $2K_{s,j} \gg KJ_{ji}$, the phase can be maintained at $\epsilon_j \approx \{-\frac{\pi}{2}, \frac{\pi}{2}\}$. These assumptions are further validated through simulations presented in the following section.

V. DESIGNING ANALOG P-BIT ENGINE

Based on the analysis above, OIMs can be configured to operate as p-bit engines using the scheme described in algorithm I. Although the analysis above was conducted in a rotated frame of reference, we present the operational details in terms of the original phase variable ϕ, to maintain consistency with the prevailing conventions in the OIM literature, where the spin states are defined as $\phi \in \{0, \pi\}$. As previously noted, the relationship between the two frames is given by $\phi = \frac{\pi}{2} + \epsilon$.

As an illustrative example, we now employ this scheme to solve the archetypal MaxCut problem in the OIM's stochastic sampling mode. Computing the MaxCut of a graph is a NP-hard problem where the objective is to partition the nodes such that the weight of the edges shared among the two sets (i.e., intersect the cut) is maximized. The MaxCut problem directly maps to the solution of the corresponding anti-ferromagnetic Ising Hamiltonian i.e., $J_{ij} = -W_{ij}$, where W_{ij} represents the weight of the edges in the graph to be partitioned.

We demonstrate this using a randomly generated graph with 15 nodes and 59 edges. Figure 3(a) illustrates the sequence of FHI^0 inputs applied to various

Algorithm I Operating OIM as a p-bit platform

1: **Initialize** all oscillators.
2: **Apply** SHI signal to all oscillators. The OIM performs gradient descent and achieves a steady state characterized by $\phi \in \{0, \pi\}$.
3: **while** not converged or for a fixed number of iterations **do**
4: Randomly select an oscillator i.
   {Step (i): Prepare oscillator for stochastic sampling}
5: Apply FHI^0 signal to oscillator i with appropriate amplitude and set SHI signal to oscillator i to 0.
   {Step (ii): Initiate probabilistic evolution}
6: Reduce FHI^0 signal to 0.
7: Ramp SHI signal to oscillator i.
8: Let ϕ_i probabilistically relax to $\phi = 0$ or $\phi = \pi$ based on synaptic feedback from connected nodes and intrinsic noise.
9: **end while**

---

randomly sampled oscillators in a sequential manner. As described earlier, the application of the FHI^0 input is accompanied by the suppression of the corresponding SHI input (not shown in Fig. 3(a) for clarity).

The resulting phase dynamics of the oscillators are shown in Fig. 3(b), where it can be observed that a sampled oscillator is first driven to a phase of $\phi = \frac{\pi}{2}$ upon application of the FHI signal, and subsequently relaxes toward either $\phi_i = 0$ or $\phi_i = \pi$ when the SHI signal is reasserted. The direction of this phase relaxation is governed by the synaptic input and noise. Arrows in Fig. 3(b) indicate representative cases where the oscillator flips its state. It is noteworthy that in traditional OIMs, such transitions are likely to have a low probability of occurrence once all oscillator phases have settled to $\phi_i = 0$ or $\phi_i = \pi$ since $\frac{d\phi}{dt}$, which effectively represents the diving force ($-\nabla E = \frac{d\phi}{dt}$) on the oscillator phase is close to zero for all oscillators i.e., $\frac{d\phi}{dt} \approx 0$. Figure 3(c) shows the corresponding evolution of the graph cut. The red arrows in Figs. 3(c) highlight the sampling events that lead to an increase in the graph cut allowing the system to compute the optimal MaxCut.

VI. STOCHASTIC SAMPLING USING OTHER ANALOG ISING MACHINES

Beyond conventional OIMs, the proposed sampling methodology exhibits potential for generalization to a broader class of analog dynamical systems. As a case in point, we evaluate the implementation of the proposed *sampling mode* in the Dynamical Ising Machine (DIM) recently introduced by the authors [32]. Unlike the traditional Kuramoto model, which relies on phase differences, the DIM employs additive phase interactions. The DIM dynamics can be described by:
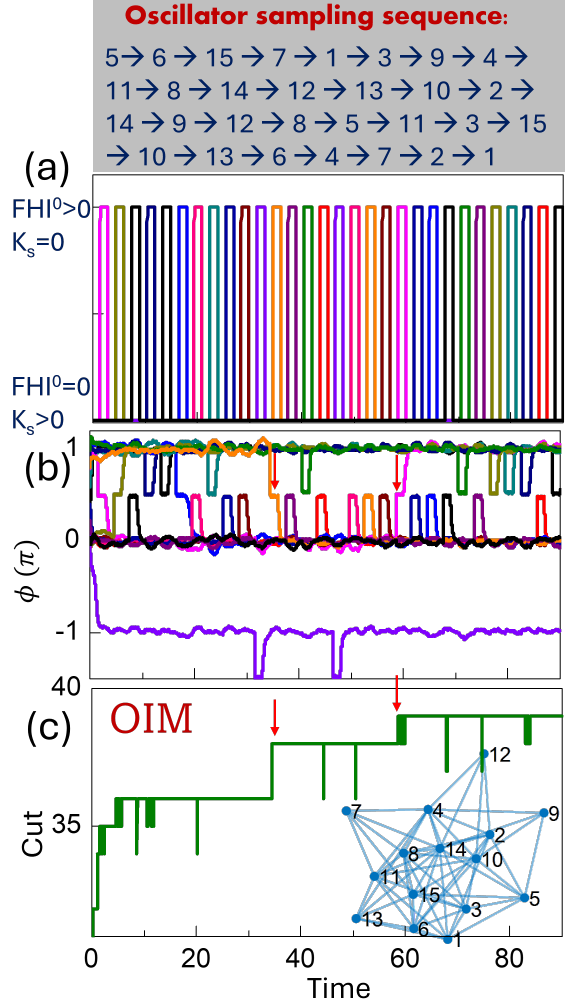

Figure 3: **Operating OIMs as p-bit platforms.** (a) Randomly generated FHI sequence to the oscillators. The application of FHI to the oscillator is accompanied by the suppression of SHI and vice-versa. (b) Phase response of the oscillators over time. (c) Evolution of the computed graph cut over time/iterations. With stochastic sampling, the system is able to reach the globally optimal solution (MaxCut =39). The red arrows highlight sampling events that improved cut ($K = 1; K_{s,\max} = 2; FHI^0 = 50; K_n$ for sampled oscillator $= 0.04$)

$$\frac{d\phi_i}{dt} = -K \sum_{\substack{j=1 \\ j \neq i}}^{N} J_{ij} \sin(\phi_i + \phi_j) - K_s \sin(2\phi_i) \quad (16)$$

Specifically, when K_s is below a certain threshold, the system stabilizes at the trivial state $\phi = \frac{\pi}{2}$. As K_s increases beyond this threshold, the system undergoes a bifurcation, leading to the emergence of stable phase configurations at $\phi \in \{0, \pi\}^N$, which can subsequently be
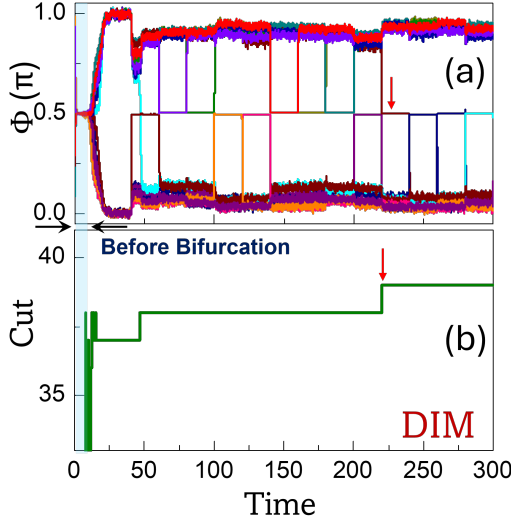
Figure 4: **Operating DIMs as p-bit platforms.** Evolution of (a) phases in the DIM model; and (b) corresponding graph cut over time. The same graph shown in Fig. 3 has been considered in the simulation. With stochastic sampling, the system is able to compute the MaxCut (=39) ($K = 1$; $K_{s,\max} = 4$; $K_c = 50$; K_n for sampled oscillator $= 0.006$).

mapped to a spin configuration. The phase dynamics of the DIM, without stochastic sampling, are presented in Appendix F for the graph considered in Fig. 3 .

While a detailed analysis of the DIM dynamics has been presented in [32], it is worth noting that the system exhibits a pitchfork bifurcation, qualitatively similar to that observed in the other popular Ising machine models such as the simulated bifurcation machine (SBM) [33]. This similarity suggests the feasibility of performing stochastic sampling in a broad class of analog dynamical systems beyond the OIM.

Similar to the OIM, the DIM dynamics in the rotated frame of reference are given by,

$$\frac{d\epsilon_i}{dt} = K \sum_{\substack{j=1 \\ j \neq i}}^{N} J_{ij} \sin(\epsilon_i + \epsilon_j) + K_s \sin(2\epsilon_i)$$

$$= \cos(\epsilon_i) \left(K \sum_{\substack{j=1 \\ j \neq i}}^{N} J_{ij} \sin(\epsilon_j) \right) + K_s \sin(2\epsilon_i) \qquad (17)$$

$$\equiv -\gamma_i \cos(\epsilon_i) + K_s \sin(2\epsilon_i)$$

where γ_i has the same definition and meaning as that in the case of the OIM. Moreover, equation (17) is exactly the same as the corresponding equation (11) derived for the OIM. Therefore, by employing the same approach

and constraints used for the OIM, the updated spin state using the DIM can be derived as follows:

$$s_i^+ \approx -\text{sgn}\left[\tanh(-\gamma_i \Delta t) + \epsilon^\eta(\Delta t).\text{sech}^2(\gamma \Delta t)\right]$$

$$\approx \text{sgn}\left[\tanh\left(K\Delta t \sum_{\substack{j=1 \\ j \neq i}}^{N} J_{ij}s_j\right) - \vartheta\right] \qquad (18)$$

Figure 4 presents a simulation demonstrating the operation of the DIM in sampling mode to compute the Max-Cut of the same graph considered in Fig. 3. As shown in Fig. 4(a), the phase dynamics initially exhibit a bifurcation as K_s is ramped up from $K_s = 0$ to $K_s = 4$ (not shown in the figure). At this stage, however, the system has not yet reached the optimal solution. With the onset of stochastic sampling, the system begins to sample the solution space and eventually converges to the optimal MaxCut value of 39, as shown in Fig. 4(b).

VII. CONCLUSION

This work builds a conceptual bridge between two paradigms that have traditionally been regarded distinct: analog oscillator-based Ising machines (OIMs) and stochastic sampling-based p-bit engines. By leveraging the natural dynamics of coupled oscillators—specifically through the interplay of SHI and FHI signals—we demonstrate that analog OIMs can perform stochastic sampling without requiring explicit computation of energy functions or the synaptic feedback. An intrinsic feature of this approach is the initial phase evolution, during which the oscillator network naturally performs gradient descent that involves the oscillator phases evolving simultaneously. Starting from random initial conditions, the phases converge to discrete states ($\phi_i \approx 0$ or $\phi_i \approx \pi$), effectively settling into a local minimum of the Ising energy landscape. This simultaneous evolution has the potential to offer a potential speed-up, positioning the system in a low-energy configuration even before the onset of the sampling-mode operation. However, these promising features come with the trade-off of requiring physical connectivity among oscillators—digital p-bit designs are better suited to implement the interaction between p-bits. From an implementation standpoint, this makes the analog approach better suited for sparse architectures. Nevertheless, this requirement aligns with the operational regimes where traditional p-bit platforms are expected to perform well. It is also important to recognize that the oscillator dynamics discussed above are valid only under specific assumptions, such as weak coupling. Furthermore, the current analysis does not account for the effects of parameter variations or frequency mismatches—factors that will be systematically explored in future work.

The overlaps between the analog and probabilistic paradigms identified in this work motivate the extension of this framework to more generalized computational models, including higher-order Ising machines [34, 35], p-bits with more than two states [19, 36], as well as to other analog systems [33, 37–41] beyond those explored here.

ACKNOWLEDGEMENTS

APPENDIX A: INJECTION LOCKING IN SINGLE OSCILLATOR

We analyze the impact of FHI on oscillator dynamics from an energy-based perspective. For an oscillator driven by an FHI signal at its natural frequency but with a phase offset θ, the phase dynamics can be described using Adler's equation [30, 31] as follows:

$$\frac{d\phi}{dt} = -K_c \sin(\phi - \theta) \tag{A1}$$

The corresponding energy function that the above dynamics minimize can be expressed as:

$$E(\phi) = -K_c \cos(\phi - \theta) \tag{A2}$$

For this system, the relationship $-\frac{dE}{d\phi} = \frac{d\phi}{dt}$ holds, implying that:

$$\frac{dE}{dt} = \frac{dE}{d\phi} \cdot \frac{d\phi}{dt} = -\left(\frac{d\phi}{dt}\right)^2 \leq 0$$

Thus, the energy monotonically decreases over time, and the system evolves toward a stable fixed point.

The minimum of the energy function occurs at $\phi^* = \theta$, where $\frac{dE}{dt} = 0$. Within the domain $\phi \in [\theta, \theta + 2\pi)$, the only other fixed point satisfying $\frac{dE}{dt} = \frac{d\phi}{dt} = 0$ is at $\phi^* = \theta + \pi$, which corresponds to a local maximum, and is therefore unstable. For all other values of ϕ in this domain, $\frac{dE}{dt} < 0$. Consequently, the oscillator phase converges to the stable fixed point $\phi = \theta$, although perturbations may be necessary to prevent the dynamics from settling at the unstable fixed point $\phi^* = \theta + \pi$.

APPENDIX B: STABILITY OF THE FIXED POINTS OF THE DYNAMICS

We analyze the stability of the fixed points associated with the dynamics described in Eq. (5) of the main text.

As previously discussed, the fixed points of the dynamics are given by, $\epsilon_1^* = \pm\frac{\pi}{2}$ and $\sin(\epsilon_2^*) = \frac{\gamma_i}{2K_s}$.

To investigate the local stability of the system, we analyze the sign of the second derivative:

$$H(\epsilon_i) = \frac{d^2\epsilon_i}{dt^2} = \gamma_i \sin(\epsilon_i) + 2K_s \cos(2\epsilon_i)$$

We seek conditions under which $H(\epsilon_i) < 0$, indicating local stability.

- **Stability of $\epsilon_1^* = \frac{\pi}{2}$**

  At this point, $\sin(\epsilon_1^*) = 1$, $\cos(2\epsilon_1^*) = -1$, so:

  $$H(\epsilon_1^*) = \gamma_i + (-2K_s) = \gamma_i - 2K_s$$

  Hence, $H(\epsilon_1^*) < 0$ when $\gamma_i < 2K_s$.

- **Stability of $\epsilon_1^* = -\frac{\pi}{2}$**

  Here, $\sin(\epsilon_1^*) = -1$, $\cos(2\epsilon_1^*) = -1$, therefore:

  $$H(\epsilon_1^*) = -\gamma_i - 2K_s$$

  Thus, $H(\epsilon_1^*) < 0$ when $\gamma_i + 2K_s > 0$.

- **Combined Condition:**

  Both fixed points $\epsilon_1^* = \pm\frac{\pi}{2}$ are stable when:

  $$\gamma_i^2 < 4K_s^2$$

- **Stability of $\sin(\epsilon_2^*) = \frac{\gamma_i}{2K_s}$**

  Substituting into $H(\epsilon_i)$, we find that:

  $$H(\epsilon_2^*) < 0 \quad \text{when} \quad \gamma_i^2 > 4K_s^2$$

APPENDIX C: TUNING ENERGY BARRIER WITH SHI STRENGTH (K_s)

We analyze the impact of K_s on the energy barrier. The function corresponding to the dynamics described by Eq. (5) is,

$$E = \gamma \sin(\epsilon) + \frac{1}{2}K_s \cos(2\epsilon) \tag{C1}$$

Figure 5 shows the resulting energy landscape for different values of K_s ($\gamma = 0$). The energy difference between the peak energy (at $\epsilon = 0$) and either valley (at $\epsilon = \pm\frac{\pi}{2}$) is given by $(\Delta E)_{max} = |K_s|$.
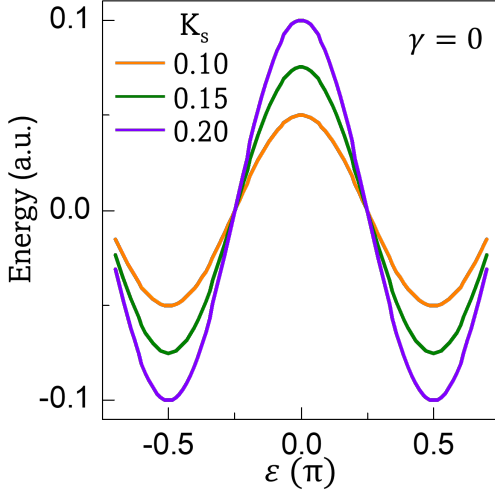
Figure 5: **Tuning energy barrier with K_s.** Evolution of the energy barrier with K_s

APPENDIX D: TEMPORAL EVOLUTION OF THE PHASE

We now analyze the dynamics presented in Eq. (5). The implicit analytical solution is given by,

$$\frac{\zeta(\epsilon) - \gamma \tanh^{-1}(\sin(\epsilon))}{\gamma^2 - 4K_s^2} = t + C \qquad \text{(D1)}$$

where,

$$\zeta(\epsilon) = K_s \big(-2 \log(\gamma - 2K_s \sin(\epsilon)) + \log(1 - \sin(\epsilon)) + \log(\sin(\epsilon) + 1) \big)$$

and C is the constant of integration. $C = 0$ since $\epsilon(t = 0) = 0$.

We now analyze the dynamics under the constraints specified in the main text, which are also restated below for reference:

(i) The dynamics are evaluated in the limit $t \to 0$.

(ii) We model the noise as Gaussian white noise with $\langle \eta(t) \rangle = 0$, $\langle \eta(t)\eta(t') \rangle = 2K_n \delta(t - t')$, with K_n denoting the noise intensity i.e., $\eta(t)\,dt = \sqrt{2K_n}\,dW_t$, where W_t is a Wiener process. Equivalently, over a finite timestep Δt, $\int_t^{t+\Delta t} \eta(\tau)\,d\tau \sim \mathcal{N}(0, 2K_n \Delta t)$.

(iii) At the onset of sampling $(t \to 0)$, we assume $K_s \to 0$ such that $K_s \ll |\gamma|$. This reflects the requirement for a low energy barrier in the probabilistic regime.

Eq. (D1) can be rearranged to yield,

$$\sin(\epsilon_i) = \tanh\left(-\gamma t + \frac{4K_s^2 t + \zeta(\epsilon)}{\gamma} + \epsilon^\eta(t) \right)$$

$$\text{(D2)}$$

$$= \tanh\left(-\gamma t + \frac{4K_s^2 t + \zeta(\epsilon)}{\gamma} + \epsilon^\eta(t) \right)$$

Here, $\epsilon^\eta(t)$ represents the perturbation induced by noise. We note that in the above analysis, we approximate the impact of noise as phase jitter; a more exhaustive treatment would model the phase dynamics as a stochastic differential equation.

From the above equation, we group all the terms dependent on K_s as,

$$\Theta = \frac{4K_s^2 t + \zeta(\epsilon)}{\gamma}$$

$$\Rightarrow \quad \sin(\epsilon_i) = \tanh\left(-\gamma t + \Theta + \epsilon^\eta(t) \right)$$

and evaluate Θ under the constraints stated above. We begin by simplifying the following terms:

$$\log(1 - \sin(\epsilon)) + \log(1 + \sin(\epsilon)) = \log(\cos^2(\epsilon)).$$

Thus, $\zeta(\epsilon) = 2K_s \left(\log\left(\cos(\epsilon)\right) - \log\left(\gamma - 2K_s \sin(\epsilon)\right) \right)$

Next, we apply the following approximations (applicable under the constraints stated above):

- $\cos(\epsilon) \approx 1 - \frac{\epsilon^2}{2} \Rightarrow \log(\cos\epsilon) \approx -\frac{\epsilon^2}{2}$

- $\sin(\epsilon) \approx \epsilon$

- $\log(\gamma - 2K_s \sin\epsilon) \approx \log|\gamma| - \frac{2K_s}{\gamma}\epsilon$

Substituting these approximations into expression for ζ yields,

$$\zeta \approx 2K_s \left(\frac{-\epsilon^2}{2} - \log(|\gamma|) + \frac{2K_s \epsilon}{\gamma} \right)$$

Subsequently, the expression Θ can be approximated as,

$$\Theta = \frac{4K_s^2 t + 2K_s \left(\frac{-\epsilon^2}{2} - \log(|\gamma|) + \frac{2K_s \epsilon}{\gamma} \right)}{\gamma}$$

$$= \frac{4K_s^2 t}{\gamma} - \frac{K_s \epsilon^2}{\gamma} - \frac{2K_s \log(|\gamma|)}{\gamma} + \frac{4K_s^2 \epsilon}{\gamma^2}$$

The above expression shows the leading-order behavior of terms dependent on K_s in the phase behavior. Moreover, when $K_s \to 0$ such that $K_s \ll |\gamma|$, $\Theta \to 0$. Nevertheless it is important that the system parameters be carefully designed to ensure that the dynamics emulate Boltzmann sampling as close as possible.
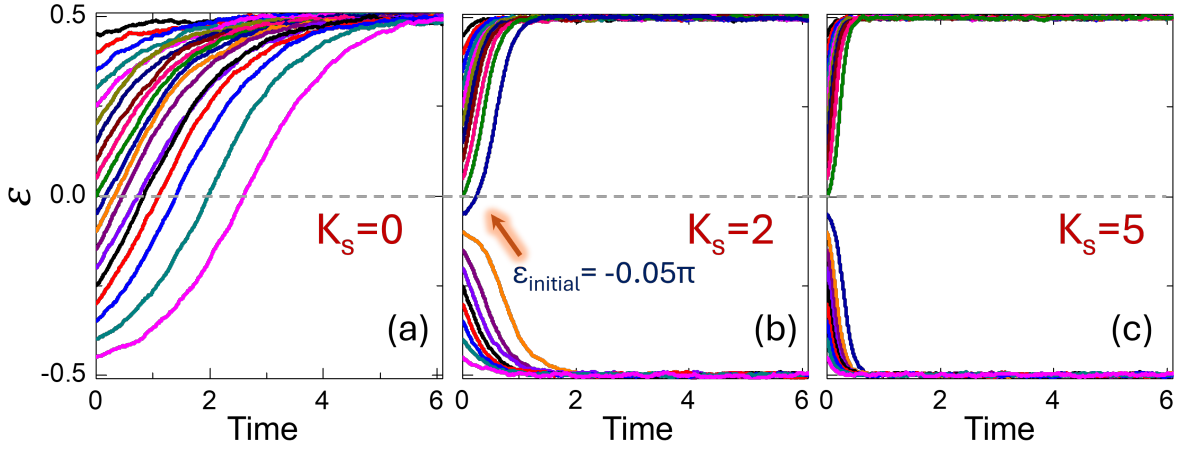
Figure 6: **Role of SHI in maintaining phase trajectory.** Phase deviation ϵ as a function of time for: (a) $K_s=0$; (b) $K_s=2$; (c) $K_s = 5$. The results in the illustrative example show that a critical SHI is needed to help the oscillator phase continue to evolve along the direction of its initial perturbation. $|\gamma_1| = 1$ has been considered in this example.

Under these conditions, Eq. (D2) can be approximated as,

$$\sin(\epsilon_i) \approx \tanh\left(-\gamma t + \epsilon^\eta(t)\right)$$

$$\approx \tanh\left(-\gamma t\right) + \epsilon^\eta(t).\mathrm{sech}^2(\gamma t)$$

Here, $\epsilon^\eta(t) \sim \mathcal{N}\left(0, 2K_n t\right)$, and is small such that the $\tanh(.)$ term can be linearized. The noise term, $\epsilon^\eta(t).\mathrm{sech}^2(\gamma t)$, can be considered as a gaussian distribution representing white noise, and scaled by a function of the synaptic input—$\mathrm{sech}^2(\gamma t)$. The updated spin state, $s^+ = -\mathrm{sgn}\left(\sin(\epsilon^+)\right)$, at a short time instant $\Delta t \to 0$ after sampling has been initiated (at $t = 0$), can be expressed as,

$$s^+ \approx \mathrm{sgn}\left[\tanh(\gamma\Delta t) - \epsilon^\eta(\Delta t).\mathrm{sech}^2(\gamma\Delta t)\right]$$

$$\equiv \mathrm{sgn}\left[\tanh(\gamma\Delta t) - \vartheta\right]$$

where, $\vartheta \equiv \epsilon^\eta(\Delta t).\mathrm{sech}^2(\gamma\Delta t)$. Since $\mathrm{sech}^2(\gamma\Delta t) \in (0,1]$, and noise power is assumed to be small, ϑ has a high probability of being in the interval [-1,+1]. We also note that for $\Delta t \to 0$, $\mathrm{sech}^2(\gamma\Delta t) \to 1 \Rightarrow \vartheta \approx \epsilon^\eta(\Delta t)$. We note that the gaussian distribution is more representative of the thermal noise found in physical devices.

We also consider the case when both γ and K_s are small. Under this assumption, the dynamics for $\epsilon \ll 1$ can be approximated as,

$$\frac{d\epsilon}{dt} \approx -\gamma + 2K_s\epsilon$$

Unlike the previous case, using the SDE framework here yields a tractable and elegant solution that offers a clear and intuitive picture of the relative competition between the stochastic and deterministic components.

We begin by considering the linear Itô SDE

$$d\varepsilon(t) = \left(-\gamma + 2K_s\epsilon(t)\right) dt + \sqrt{2K_n}\, dW_t,$$
(D3)

where we note that $\epsilon(0) = 0$, $K_s > 0$.

Integrating factor: Let $M(t) = e^{-2K_s t}$. Since M is deterministic,

$$d\left(M(t)\epsilon(t)\right) = M(t)\, d\epsilon(t) + \epsilon(t)\, dM(t)$$
$$= -\gamma M(t)\, dt + \sqrt{2K_n}\, M(t)\, dW_t. \quad \text{(D4)}$$

Integration from 0 to t yields

$$M(t)\epsilon(t) = -\gamma \int_0^t M(s)\, ds$$
$$+ \sqrt{2K_n} \int_0^t M(s)\, dW_s. \quad \text{(D5)}$$

Since

$$\int_0^t e^{-2K_s s}\, ds = \frac{1 - e^{-2K_s t}}{2K_s}, \quad M(t)^{-1} = e^{2K_s t},$$

we obtain

$$\epsilon(t) = \frac{\gamma}{2K_s}\left(1 - e^{2K_s t}\right) + \sqrt{2K_n} \int_0^t e^{2K_s(t-s)}\, dW_s. \quad \text{(D6)}$$

Mean: The stochastic integral in (D6) has zero mean:

$$\mathbb{E}[\epsilon(t)] = \frac{\gamma}{2K_s}\left(1 - e^{2K_s t}\right). \quad \text{(D7)}$$

Variance: By Itô isometry,

$$\mathrm{Var}[\epsilon(t)] = 2K_n \int_0^t e^{4K_s(t-s)}\, ds$$
$$= \frac{K_n}{2K_s}\left(e^{4K_s t} - 1\right). \quad \text{(D8)}$$

The above results imply that for $K_s > 0$, both mean and variance diverge exponentially. Thus, no stationary distribution exists. Two limiting cases further clarify the dynamics:

- **Case $\gamma = 0$.** In the absence of the synaptic input, the deterministic contribution reduces to $d\epsilon = 2K_s\epsilon\, dt$. With $\epsilon(0) = 0$, this term alone would maintain $\epsilon(t) \equiv 0$. However, in the presence of Gaussian noise, random perturbations are continuously injected and then exponentially amplified by the unstable drift. Consequently, the growth of $\epsilon(t)$ is seeded by stochastic fluctuations and deterministically amplified over time.

- **Case $\gamma \neq 0$.** When $\gamma \neq 0$, both deterministic and stochastic contributions govern the dynamics. As seen from Eq. (D7) and Eq. (D8), both the drift-induced component and the noise-driven fluctuations diverge as t increases. The relative dominance of these two effects depends on the balance between the deterministic drive, set by $|\gamma|$, and the stochastic forcing, quantified by K_n. A stronger deterministic bias leads to more predictable exponential growth, whereas larger noise intensity results in greater dispersion across trajectories.

APPENDIX E: ROLE OF SHI DURING STOCHASTIC SAMPLING

To analyze how the SHI can help the oscillator maintain the phase trajectory resulting from the stochastic sampling process, we examine Eq. (5):

$$\frac{d\epsilon}{dt} = -\gamma\cos(\epsilon) + K_s\sin(2\epsilon)$$

As discussed in the main text, the role of SHI is particularly critical when the initial direction of phase relaxation is counter to that expected from synaptic feedback, owing to noise. As noted earlier, the synaptic input (alone) tends to push the phase toward the fixed point opposite to the sign of γ. In other words, we seek to analyze the conditions under which the initial flow of the dynamics is towards $\epsilon = +\frac{\pi}{2}(-\frac{\pi}{2})$, even when though the synaptic input is $\gamma > 0$ $(\gamma < 0)$, respectively.

Assuming that the initial perturbation results in a phase magnitude given by $|\epsilon_{th}|$, the critical condition on K_s to ensure that the phase continues to flow in the same direction can be expressed as,

$$2K_s\sin(|\epsilon_{th}|) > |\gamma| \tag{E1}$$

This condition ensures the RHS of Eq. (5) maintains the same sign as the phase at $\epsilon = \epsilon_{th}$. Further, since $\sin(.)$ is monotonic in the region, $|\epsilon| \in \{0, \frac{\pi}{2}\}$, the sign of the RHS terms will not change until dynamics reach the corresponding fixed point. We note that in the presence of noise, the above condition should be interpreted in a probabilistic sense.

We also illustrate this behavior using a simple example: a negatively coupled two-oscillator system (with $K = 1$) in which the phase of oscillator 2 is fixed at $\epsilon_2 = -\frac{\pi}{2}$ yielding $\gamma_1 = -1 \Rightarrow |\gamma_1| = 1$. In this configuration, the energetically favorable state for oscillator 1 is $\epsilon_1 = \frac{\pi}{2}$, and synaptic feedback is expected to drive the system toward this fixed point. To explore the system's dynamics, oscillator 1 is initialized at various discrete phase values within the range $\epsilon_{th} \in [-0.45\pi, 0.45\pi]$. Figures 6(a–c) show the evolution of ϵ for different values of K_s.

In the absence of synaptic hysteresis (i.e., $K_s = 0$), the phase does not preserve the direction of its initial perturbation. Instead, it eventually aligns with the direction of the synaptic input, converging to $\epsilon = \frac{\pi}{2}$. This behavior is expected, as the inequality in Eq. (E1) is never satisfied in this regime.

Introducing SHI (i.e., $K_s > 0$) enables the oscillator phase to continue evolving along the direction of ϵ_{th}. However, the magnitude of K_s must exceed a certain threshold. This behavior is illustrated in Figs. 6(b) and 6(c). In Fig. 6(b), when K_s is below the threshold required for that $\epsilon_{th} = -0.05\pi$, the phase evolution eventually aligns with the direction favored by the synaptic input. In contrast, when K_s is sufficiently, as in Fig. 6(c)), all initial phase values considered here evolve along the direction of their original perturbation. Thus, the SHI injection strength, K_s, must be carefully engineered to ensure that one phase magnitudes beyond a certain threshold evolve continue to evolve in the direction of their initial perturbation.
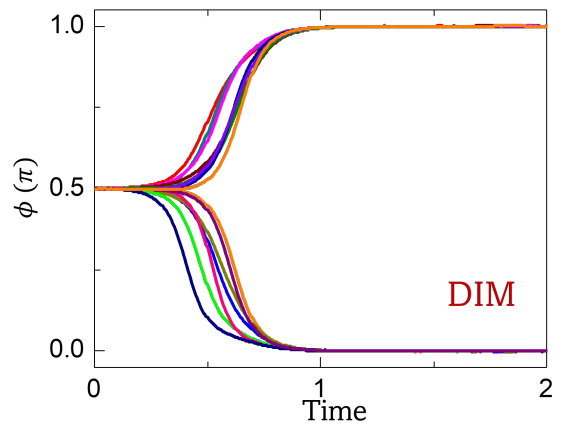
APPENDIX F: DYNAMICS OF DYNAMICAL ISING MACHINE

Figure 7: **Dynamical Ising Machine.** Evolution of ϕ in the DIM model for the graph considered in Fig. 3 (K=1; $K_s(t) = 0.4t$; $K_n = 0.002$).

Figure 7 evaluates the graph considered in Fig. 3 using

the analog dynamics of the DIM (without stochastic sampling). A bifurcation similar to that exhibited by other models such as SBM [33] is observed.

REFERENCES

[1] N. Mohseni, P. L. McMahon, and T. Byrnes. Ising machines as hardware solvers of combinatorial optimization problems. *Nature Reviews Physics* **4**(6), 363–379 (2022).

[2] R. Hamerly, T. Inagaki, P. L. McMahon, D. Venturelli, A. Marandi, T. Onodera, E. Ng, C. Langrock, K. Inaba, T. Honjo, *et al.* Experimental investigation of performance differences between coherent Ising machines and a quantum annealer. *Science Advances* **5**(5), eaau0823 (2019).

[3] T. Honjo, T. Sonobe, K. Inaba, T. Inagaki, T. Ikuta, Y. Yamada, T. Kazama, K. Enbutsu, T. Umeki, R. Kasahara, *et al.* 100,000-spin coherent Ising machine. *Science Advances* **7**(40), eabh0952 (2021).

[4] A. Litvinenko, R. Khymyn, R. Ovcharov, and J. Åkerman. A 50-spin surface acoustic wave Ising machine. *Communications Physics* **8**(1), 1–11 (2025).

[5] A. Mallick, M. K. Bashar, D. S. Truesdell, B. H. Calhoun, and N. Shukla. Overcoming the accuracy vs. performance trade-off in oscillator ising machines. In *2021 IEEE International Electron Devices Meeting (IEDM)*, 40–2 (2021).

[6] W. Moy, I. Ahmed, P.-W. Chiu, J. Moy, S. S. Sapatnekar, and C. H. Kim. A 1,968-node coupled ring oscillator circuit for combinatorial optimization problem solving. *Nature Electronics* **5**(5), 310–317 (2022).

[7] M. K. Bashar, A. Mallick, D. S. Truesdell, B. H. Calhoun, S. Joshi, and N. Shukla. Experimental demonstration of a reconfigurable coupled oscillator platform to solve the max-cut problem. *IEEE Journal on Exploratory Solid-State Computational Devices and Circuits* **6**(2), 116–121 (2020).

[8] J. Vaidya, R. S. Kanthi, and N. Shukla. Creating electronic oscillator-based Ising machines without external injection locking. *Scientific Reports* **12**(1), 981 (2022).

[9] O. Maher, M. Jiménez, C. Delacour, N. Harnack, J. Núñez, M. J. Avedillo, B. Linares-Barranco, A. Todri-Sanial, G. Indiveri, and S. Karg. A CMOS-compatible oscillation-based VO₂ Ising machine solver. *Nature Communications* **15**(1), 3334 (2024).

[10] H. Cılasun, W. Moy, Z. Zeng, T. Islam, H. Lo, A. Vanasse, M. Tan, M. Anees, A. Kumar, S. S. Sapatnekar, *et al.* A coupled-oscillator-based Ising chip for combinatorial optimization. *Nature Electronics* 1–10 (2025).

[11] A. Litvinenko, R. Khymyn, V. H. González, R. Ovcharov, A. A. Awad, V. Tyberkevych, A. Slavin, and J. Åkerman. A spinwave Ising machine. *Communications Physics* **6**(1), 227 (2023).

[12] A. D. King, S. Suzuki, J. Raymond, A. Zucca, T. Lanting, F. Altomare, A. J. Berkley, S. Ejtemaee, E. Hoskinson, S. Huang, *et al.* Coherent quantum annealing in a programmable 2,000 qubit Ising chain. *Nature Physics* **18**(11), 1324–1328 (2022).

[13] T. Wang, L. Wu, P. Nobel, and J. Roychowdhury. Solving combinatorial optimisation problems using oscillator based Ising machines. *Natural Computing* **20**(2), 287–306 (2021).

[14] M. K. Bashar, Z. Lin, and N. Shukla. Stability of oscillator Ising machines: Not all solutions are created equal. *J. Appl. Phys.* **134**(14), 144901 (2023).

[15] Y. Cheng, M. K. Bashar, N. Shukla, and Z. Lin. A control theoretic analysis of oscillator Ising machines. *Chaos: An Interdisciplinary Journal of Nonlinear Science* **34**(7) (2024).

[16] A. Allibhoy, A. N. Montanari, F. Pasqualetti, and A. E. Motter. Global Optimization Through Heterogeneous Oscillator Ising Machines. *arXiv preprint* arXiv:2505.17027 (2025).

[17] N. A. Aadit, A. Grimaldi, M. Carpentieri, L. Theogarajan, J. M. Martinis, G. Finocchio, and K. Y. Camsari. Massively parallel probabilistic computing with sparse Ising machines. *Nature Electronics* **5**(7), 460–468 (2022).

[18] S. Chowdhury, A. Grimaldi, N. A. Aadit, S. Niazi, M. Mohseni, S. Kanai, H. Ohno, S. Fukami, L. Theogarajan, G. Finocchio, *et al.* A full-stack view of probabilistic computing with p-bits: Devices, architectures, and algorithms. *IEEE Journal on Exploratory Solid-State Computational Devices and Circuits* **9**(1), 1–11 (2023).

[19] W. Whitehead, Z. Nelson, K. Y. Camsari, and L. Theogarajan. CMOS-compatible Ising and Potts annealing using single-photon avalanche diodes. *Nature Electronics* **6**(12), 1009–1019 (2023).

[20] C. Duffee, J. Athas, Y. Shao, N. D. Melendez, E. Raimondo, J. A. Katine, K. Y. Camsari, G. Finocchio, and P. K. Amiri. Integrated probabilistic computer using voltage-controlled magnetic tunnel junctions as its entropy source. *arXiv preprint* arXiv:2412.08017 (2024).

[21] W. A. Borders, A. Z. Pervaiz, S. Fukami, K. Y. Camsari, H. Ohno, and S. Datta. Integer factorization using stochastic magnetic tunnel junctions. *Nature* **573**(7774), 390–393 (2019).

[22] N. S. Singh, K. Kobayashi, Q. Cao, K. Selcuk, T. Hu, S. Niazi, N. A. Aadit, S. Kanai, H. Ohno, S. Fukami, *et al.* CMOS plus stochastic nanomagnets enabling heterogeneous computers for probabilistic inference and learning. *Nature Communications* **15**(1), 2685 (2024).

[23] J. Si, S. Yang, Y. Cen, J. Chen, Y. Huang, Z. Yao, D.-J. Kim, K. Cai, J. Yoo, X. Fong, *et al.* Energy-efficient superparamagnetic Ising machine and its application to traveling salesman problems. *Nature Communications* **15**(1), 3457 (2024).

[24] J. Jhonsa, W. Whitehead, D. McCarthy, S. Chowdhury, K. Camsari, and L. Theogarajan. A CMOS Probabilistic Computing Chip With In-situ hardware Aware Learning. *arXiv preprint* arXiv:2504.14070 (2025).

[25] K. Y. Camsari, B. M. Sutton, and S. Datta. P-bits for probabilistic spin logic. *Applied Physics Reviews* **6**(1) (2019).

[26] K. Y. Camsari, R. Faria, B. M. Sutton, and S. Datta. Stochastic p-bits for invertible logic. *Physical Review X* **7**(3), 031014 (2017).

[27] F. Böhm, D. Alonso-Urquijo, G. Verschae, and G. Van der Sande. Noise-injected analog Ising machines enable ultrafast statistical sampling and machine learning. *Nature Communications* **13**(1), 5847 (2022).

[28] K. Lee, S. Chowdhury, and K. Y. Camsari. Noise-augmented chaotic Ising machines for combinatorial optimization and sampling. *Communications Physics* **8**(1), 35 (2025).

[29] R. Faria, K. Y. Camsari, and S. Datta. Low-barrier nano-magnets as p-bits for spin logic. *IEEE Magnetics Letters* **8**, 1–5 (2017).

[30] R. Adler. A study of locking phenomena in oscillators. *Proceedings of the IRE* **34**(6), 351–357 (2006).

[31] P. Bhansali and J. Roychowdhury. Gen-Adler: The generalized Adler's equation for injection locking analysis in oscillators. In *2009 Asia and South Pacific Design Automation Conference*, 522–527 (2009).

[32] E. M. H. E. B. Ekanayake and N. Shukla. Different paths, same destination: Designing physics-inspired dynamical systems with engineered stability to minimize the Ising Hamiltonian. *Phys. Rev. Appl.* **24**(2), 024008 (2025).

[33] H. Goto, K. Tatsumura, and A. R. Dixon. Combinatorial optimization by simulating adiabatic bifurcations in nonlinear Hamiltonian systems. *Science Advances* **5**(4), eaav2372 (2019).

[34] M. K. Bashar and N. Shukla. Designing Ising machines with higher order spin interactions and their application in solving combinatorial optimization. *Scientific Reports* **13**(1), 9558 (2023).

[35] D. Kleyko, D. Nikonov, A. Khosrowshahi, B. Olshausen, C. Bybee, and F. Sommer. Efficient optimization with higher-order ising machines. *Nature Communications* **14**(1) (2023).

[36] C. Duffee, J. Athas, A. Grimaldi, D. Volpe, G. Finocchio, E. Wei, and P. K. Amiri. Extended-variable probabilistic computing with p-dits. *arXiv preprint* arXiv:2506.00269 (2025).

[37] M. Honari-Latifpour and M.-A. Miri. Optical Potts machine through networks of three-photon down-conversion oscillators. *Nanophotonics* **9**(13), 4199–4205 (2020).

[38] N. Berloff and J. Cummins. Vector Ising Spin Annealer for Minimizing Ising Hamiltonians. (2025), Nature Portfolio.

[39] A. Mallick, M. K. Bashar, Z. Lin, and N. Shukla. Computational models based on synchronized oscillators for solving combinatorial optimization problems. *Physical Review Applied* **17**(6), 064064 (2022).

[40] C. Delacour, B. Haverkort, F. Sabo, N. Azemard, and A. Todri-Sanial. Lagrange Oscillatory Neural Networks for Constraint Satisfaction and Optimization. *arXiv preprint* arXiv:2505.07179 (2025).

[41] M. Ercsey-Ravasz and Z. Toroczkai. Optimization hardness as transient chaos in an analog approach to constraint satisfaction. *Nature Physics* **7**(12), 966–970 (2011).